CRYSTAL GROWTH & DESIGN

pubs.acs.org/crystal

Article

Mechanosynthesis, Characterization, and Physicochemical Property Investigation of a Favipiravir Cocrystal with Theophylline and GRAS Coformers

Published as part of a Crystal Growth and Design virtual special issue on Emerging Investigators 2022.

Poonam Deka,[‖] Diptajyoti Gogoi,[‖] Khaled Althubeiti, Dharmaraj R. Rao, and Ranjit Thakuria*

Cite This: *Cryst. Growth Des.* 2021, 21, 4417−4425

Read Online

ACCESS | Metrics & More | Article Recommendations | Supporting Information

ABSTRACT: Five cocrystals of antiviral drug favipiravir (Fav) with respiratory drug theophylline (Theo) and GRAS coformers, viz., *p*-aminobenzoic acid (PABA), 4-hydroxybenzoic acid (4HBA), gallic acid (GA), and ferulic acid (FRA), were successfully synthesized using mechanochemistry as well as solution crystallization. All the synthesized cocrystals were characterized using PXRD, SCXRD, and thermal analysis. A physicochemical property investigation showed an excellent correlation of coformer solubility with cocrystal solubility. Moreover, cocrystal solubility can be tuned based on the selection of coformers during cocrystallization as well as the pH of the medium. Crystal structure analysis depicts amide−amide homosynthon formation in the Fav·Theo cocrystal and an acid−amide heterosynthon in the case of cocrystals with GRAS coformers. Incorporation of nutraceuticals (GA and FRA) provides an additional health benefit, whereas Fav·Theo cocrystal may be a potential formulation to treat patients suffering from chronic obstructive pulmonary disease (COPD) or asthma along with viral infections.

INTRODUCTION

6-Fluoro-3-hydroxypyrazine-2-carboxamide commercially known as favipiravir (Fav) is a new broad-spectrum antiviral drug that selectively and strongly inhibits the RNA-dependent RNA polymerase (RdRp) of RNA viruses.[1,2] It was first developed and manufactured by Toyama Chemicals in Japan during 2014 and is effective against a wide range of influenza viruses and subtypes. Fav came into much attention during the year 2020 for its use as a drug against severe acute respiratory syndrome coronavirus 2 (SARS-CoV-2) infections, more commonly known as COVID-19.[3−6] A docking study carried out by Ataseven and co-workers[7] also showed high potential of a Fav analogue against RdRp of different virus types compared to existing drug molecules such as lopinavir, ritonavir, etc. Moreover, it is also used against other viral infections like Ebola, Lassa, and Nipah in recent times.[8] The anhydrous form of Fav was first reported by Shi et al.[9] solved in the orthorhombic $Pna2_1$ space group containing one molecule in the asymmetric unit. Structure analysis showed the molecule to be nearly planar with an intramolecular O−H···O hydrogen bond in an enol-like tautomeric form (Scheme 1a). Gas phase analysis showed better stability of the enol-like form compared to the keto form.[10] During preparation of this manuscript, Vologzhanina and co-worker reported[11] a new tetragonal polymorph of Fav solved in the $P4_2/n$ space group containing an amide−pyrazine (N−H···N) hydrogen bond that connects adjacent molecules. Based on periodic density functional theory (DFT) calculation, they established the newly synthesized polymorph to be metastable in nature and readily convertible to the orthorhombic form under room temperature. Unlike its structural analogue pyrazinamide (α, β, and δ polymorphs),[12] the Fav anhydrous form does not contain the commonly encountered amide−amide dimer synthon. A Cambridge Structural Database (CSD) search (version 5.42; performed on Nov. 2020 update) on Fav multicomponent solids (salts, cocrystals, solvates, eutectics, or coamorphous) showed no results until date. Moreover, moderate solubility and a relatively unexplored physicochemical study of the anhydrous form[13] lead us to explore possible crystal structure landscape of Fav. Based on a complementary hydrogen bond, a few GRAS (generally regarded as safe) coformers (see Scheme 1b) along with theophylline (Theo), a phosphodiesterase inhibiting drug, were considered as potential coformers to

Received: March 26, 2021
Revised: July 1, 2021
Published: July 22, 2021

Downloaded via GAUHATI UNIV on August 18, 2021 at 07:39:49 (UTC).
See https://pubs.acs.org/sharingguidelines for options on how to legitimately share published articles.

ACS Publications

© 2021 American Chemical Society

https://doi.org/10.1021/acs.cgd.1c00339
Cryst. Growth Des. 2021, 21, 4417−4425

Scheme 1. (a) Possible Molecular Conformations of the Fav Anhydrous Form[a]; (b) Molecular Structures of Theo and GRAS Coformers Used in This Study

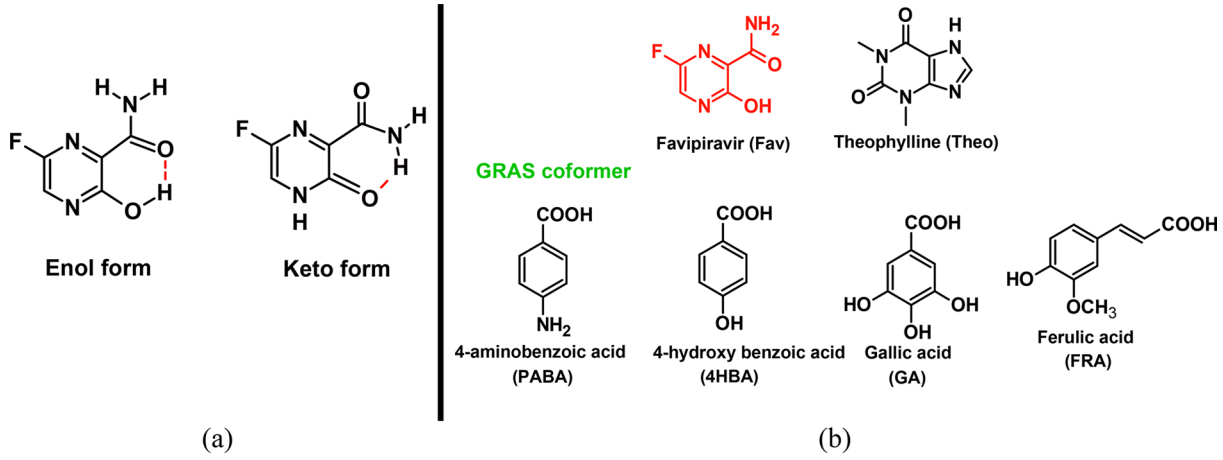

[a]Enol and keto-like forms.

synthesize cocrystals of Fav, and their physicochemical properties were investigated. Drug−drug and drug−nutraceutical cocrystals have potential application against multiple ailments, as they reduce drug load and cost effects during multiple disease diagnosis. In a recent review,[14] examples of various drug−drug and drug−nutraceuticals, their importance, synergistic effect along with their physicochemical properties were discussed in depth. As COVID-19 hits the whole world and rendering patients with comorbidities vulnerable, along with antiviral drug additional health supplements/drugs are necessary. With respect to that, our aim to develop a drug−drug cocrystal with Theo and drug−nutraceutical cocrystals with GA and FRA may have potential importance. In a recent review, Savi et al.[13] also discussed about repurposing small-molecule drugs as an active route against a search for a COVID-19 cure.

EXPERIMENTAL SECTION

Materials. Fav was a gift from Cipla Pharmaceutical Division, Mumbai, and used as received. All other coformers were purchased from local suppliers and used without further purification.

Synthesis of Fav Cocrystals. Fav (15.7 mg, 0.1 mmol) along with all other coformers in 1:1 stoichiometry were ground in a mortar pestle in the presence of 2−3 drops of acetonitrile as liquid (liquid assisted grinding, LAG) for about 15 min, resulting in the respective cocrystals. The resultant powder materials were examined using powder X-ray diffraction and thermal techniques.

Equilibrium Solubility Measurements Using UV−Visible Spectroscopy. The equilibrium solubility of Fav and all synthesized cocrystals was determined in distilled water as well as in pH 7.0 phosphate buffer at room temperature (298 K). UV−visible spectroscopy was used to measure the equilibrium solubility. Extinction coefficients (ε) were determined for all the individual solid samples using Beer−Lambert's law, $A = \varepsilon Cl$, by preparing the standard solutions and plotting the absorbance (A) vs concentration (C) curve. Equilibrium solubility values were determined using the shake-flask method[15] by stirring an excess amount of the solid sample in 5 mL of distilled water for ∼18 h or pH 7 phosphate buffer for ∼24 h at room temperature. Then, the saturated solutions were double filtered through a Whatman 42 paper and diluted to obtain an acceptable absorbance value. The concentration of the diluted solution was then multiplied by the dilution factor to calculate the equilibrium solubility of the resultant saturated solution. The residue obtained after filtration was dried under open atmosphere, and PXRD was recorded to confirm the stability of the respective powder materials. Details of the solubility parameters are listed in Supporting Information Tables S1 and S2. The coformer solubility data available in published literature is compared with the equilibrium solubility of the cocrystals in Supporting Information Table S3.

Powder X-ray Diffraction (PXRD). PXRD measurements were performed on a Rigaku Ultima IV X-ray powder diffractometer operating a Cu Kα X-ray source, equipped with a Ni filter to suppress Kβ emission and a D/teX Ultra high-speed position sensitive detector, and measurements were performed at room temperature, with a scan range 2θ = 5−50°, step size of 0.02°, and scan rate of 10° min^{-1}.

Single Crystal X-ray Diffraction (SCXRD). SCXRD data were collected on a Bruker SMART APEX II CCD diffractometer equipped with a graphite monochromator and a Mo Kα fine-focus sealed tube (λ = 0.71073 Å). Data integration was done using SAINT. Intensities for absorption were corrected using SADABS. Structure solution and refinement were carried out using Bruker SHELXTL.[16] The hydrogen atoms were refined isotropically, and all the other atoms were refined anisotropically. N−H and O−H hydrogens were located from difference electron density maps, and C−H hydrogens were fixed using the HFIX command in SHELXTL. Molecular graphics were prepared using X-SEED[17,18] and Mercury licensed version 3.0.

Thermal Analysis. Thermogravimetric (TG) measurements were performed on a Mettler Toledo instrument with a temperature range of 25−700 °C and a heating rate of 20 °C min^{-1}. Samples were placed in silica crucibles and purged by a stream of nitrogen flowing at 80 mL min^{-1}. DSC measurements were performed on a Mettler Toledo DSC instrument with a temperature range of 25−400 °C and heating rate of 10 °C min^{-1} on a 40 μL aluminum pan with a pinhole lid under an ultrahigh pure nitrogen environment purged at 40 mL min^{-1}.

FESEM Analysis. The morphology of Fav and all synthesized cocrystal powder materials prepared using LAG was analyzed using FESEM, Sigma-300, ZEISS.

RESULTS AND DISCUSSION

Apart from crystal structure analysis of the Fav anhydrous form,[9,11] no reports are available on physicochemical property study of Fav. Structural analysis and characterization of the synthesized cocrystals of Fav are discussed in the subsequent sections.

Fav·Theo Cocrystal (1:1). Crystallization of the 1:1 stoichiometric mixture of ground material Fav and Theo obtained from LAG in acetonitrile solvent afforded a needle shaped single crystal of the same. The crystal structure was solved in monoclinic space group $P2_1/n$ containing one molecule of Fav and Theo in the asymmetric unit. The *o*-

https://doi.org/10.1021/acs.cgd.1c00339
Cryst. Growth Des. 2021, 21, 4417−4425

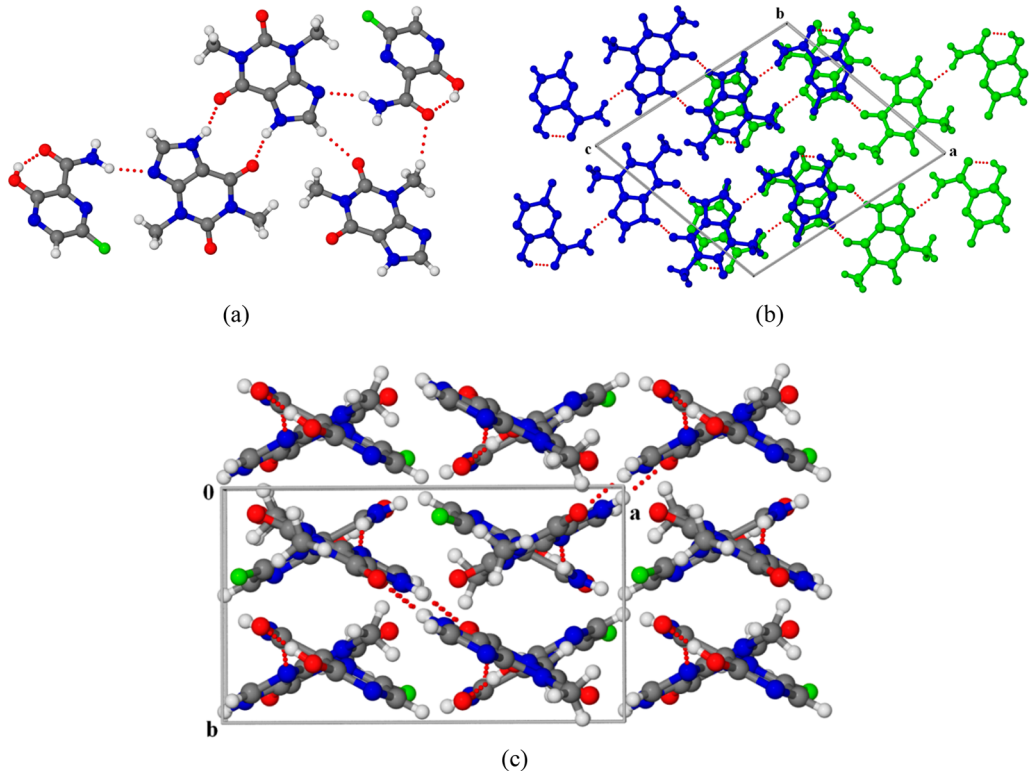

Figure 1. (a) 1D infinite chain of Fav−Theo dimers connected via a N−H···N hydrogen bond along the *c*-axis. Weak C−H···O interaction present between the adjacent molecules is also shown. (b) Stacks of 1D infinite chains of Fav−Theo along the *c*-axis connected via a van der Waals interaction. (c) Infinite chains resulted a grid-like structure viewed along the *ab*-plane.

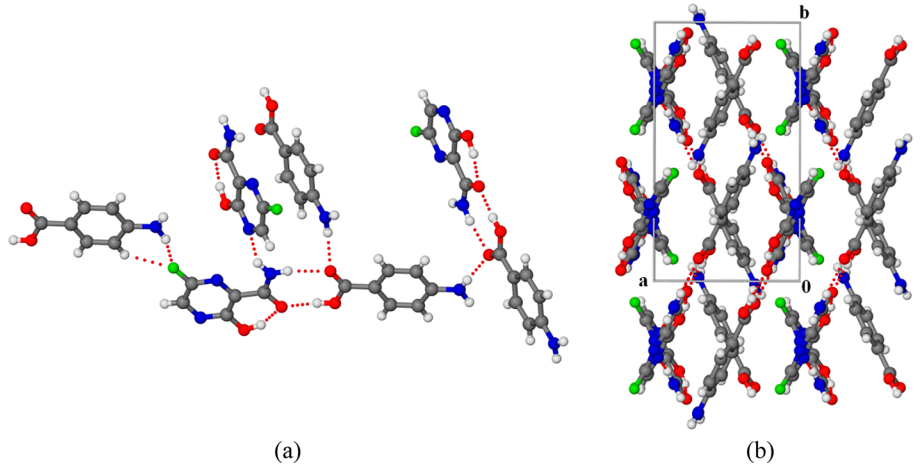

Figure 2. (a) Acid−amide heteromeric dimers of Fav−PABA connected to adjacent dimers via N−$H_{amide,Fav}$···$N_{pyrazine,Fav}$ and N−$H_{amino,PABA}$···$O_{carbonyl,PABA}$ hydrogen bonds. (b) A grid-like 3D crystal packing viewed along the *ab*-plane.

hydroxy group adjacent to the amide functional of Fav forms an intramolecular O−H···O hydrogen bond with the amide carbonyl, resulting in a six membered S(6) synthon. Two molecules of Fav are connected to each other via an amide dimer synthon $R_2^2(8)$ that further connects centrosymmetric theophylline dimers via a N−$H_{amide,Fav}$···$N_{imidazole,Theo}$ hydrogen bond forming an infinite chain along the *c*-axis, Figure 1a. These infinite chains are stacked over each other using a $\pi\cdots\pi$ interaction (Figure 1b) that results in a grid-like crystal packing as shown in Figure 1c. Due to presence of a lesser number of hydrogen bond donor sites, pyrazine Ns of Fav remain idle, and no suitable hydrogen bond interactions have been observed in the cocrystal structure. Weak C−H···O interactions involving a $carbonyl_{(urea)}$ of Theo with a neighboring C−H group of $imidazole_{(Theo)}$ (C10−H10···O3) and methyl group of Theo with a $carbonyl_{(Fav)}$ functional of an adjacent neighbor (C11−H11C···O1) have been observed that further strengthen the interaction between the cocrystal components.

Fav·PABA Cocrystal (1:1). Crystallization of 1:1 stoichiometric ground powder of Fav and PABA obtained from LAG in acetonitrile afforded a lath shaped single crystal of Fav·PABA. The crystal structure was solved in centrosymmetric $P2_1/c$ space group containing one molecule of each Fav and PABA. The crystal structure contains the most favorable acid−amide heterosynthon with graph set notation $R_2^2(8)$ between Fav and PABA (Figure 2a). This acid−amide dimer further

https://doi.org/10.1021/acs.cgd.1c00339
Cryst. Growth Des. 2021, 21, 4417−4425

connects neighboring dimers via $N-H_{amide,Fav}\cdots N_{pyrazine,Fav}$ and $N-H_{amino,PABA}\cdots O_{carbonyl,PABA}$ hydrogen bonds that result in a square grid-like crystal packing along the *ab*-plane as shown in Figure 2b. Moreover, the fluoro group of Fav forms a six membered ring synthon $R_2^1(6)$ connecting a *p*-amino group (N−H···F) and aromatic ring hydrogen (C−H···F) of an adjacent neighbor (PABA molecule).

Fav·4HBA Cocrystal (1:1). Cocrystallizing Fav with molecular analogue 4HBA resulted in a 1:1 cocrystal of Fav·4HBA similar to that of the Fav·PABA cocrystal. The block shaped single crystal of Fav·4HBA was solved in monoclinic $P2_1/c$ space group. The crystal structure contains an acid−amide dimer synthon similar to the Fav·PABA cocrystal; however, the 3D packing arrangement of the two cocrystals is quite different. The *p*-hydroxy group of 4HBA connects the pyrazine ring N of Fav ($O-H_{4HBA}\cdots N_{pyrazine,Fav}$) using a hydrogen bond that results in an infinite 1D chain along the *c*-axis (Figure 3a). Apart from these strong hydrogen bond interactions, the fluoro group of Fav connects an aromatic ring hydrogen of adjacent 4HBA using a weak C−H···F interaction. In three dimensions, these parallel 1D chains of Fav−4HBA are superimposed over each other, forming a zigzag crystal packing along the *bc*-plane as shown in Figure 3b.

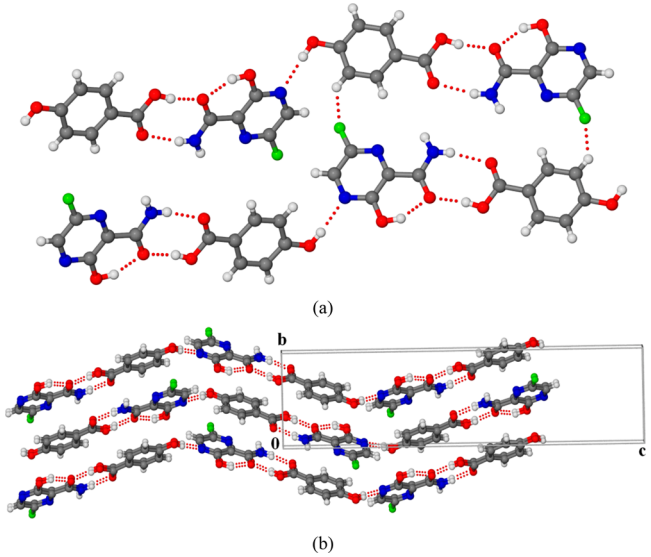

Figure 3. (a) Acid−amide dimers of Fav−4HBA further connected via an $O-H_{hydroxy}\cdots N_{pyrazine}$ hydrogen bond results a 1D chain along the *c*-axis. Adjacent chains are connected to each other using a weak C−H···F interaction. (b) Parallel chains of Fav−4HBA stacked along the *c*-axis result in a zigzag crystal packing viewed along the *bc*-plane.

Fav·GA·2H$_2$O Cocrystal (1:1:2). Crystallizing powder samples of a 1:1 Fav−GA ground mixture from acetonitrile results in a block shaped single crystal of a Fav·GA cocrystal. The crystal structure was solved in monoclinic $P2_1/n$ space group with one molecule of Fav and GA, along with two water molecules in the asymmetric unit. The crystal structure contains an acid−amide dimer synthon between GA and Fav molecules. The two water molecules present in the crystal structure balance the mismatched hydrogen bond donor−acceptor ratio. The three hydroxyl groups of GA form O−H···O hydrogen bonds connecting two symmetry-independent waters as well as the neighboring Fav−GA dimers, which result in a two-dimensional sheet structure (Figure 4a). Two water molecules sit on a tetrahedral position connecting two adjacent layers using an O−H···O hydrogen bond as shown in Figure 4b. Liquid assisted grinding (LAG) results in the formation of dihydrate cocrystal, whereas neat grinding (NG) yields a dihydrate cocrystal along with the starting materials confirmed using PXRD, which suggest better stability of the dihydrate and ready conversion of the anhydrous form (cocrystal) into its dihydrate under ambient temperature and pressure (see SI Figure S1). Presence of the two water molecules in the crystal lattice was further confirmed using thermal analysis discussed later under the Thermal Analysis section.

Fav·FRA Cocrystal (1:1). Crystallization of the 1:1 stoichiometric ground materials of Fav and FRA in acetonitrile afforded thin needle shaped single crystals of the Fav·FRA cocrystal. The crystal structure was solved in triclinic $P\bar{1}$ space group with one molecule of each Fav and FRA in the asymmetric unit. The symmetry-independent molecules are connected to each other using the most favorable acid−amide dimer synthon. Two adjacent Fav−FRA dimers are further connected via a bifurcated N−H···O hydrogen bond as shown in Figure 5a. In 3D, these discrete Fav−FRA dimers are stacked over each other in head-to-tail fashion. The *p*-hydroxyl group of FRA does not form any strong hydrogen bond, rather the *m*-methoxy group is protruding toward the molecular slips along the (001) plane connecting a neighboring hydroxyl group of Fav using weak C−H···O interactions (Figure 5b). The fluoro group of Fav forms a weak C−H···F interaction with an aromatic hydrogen of a neighboring FRA molecule. From structural analysis, it was observed that a Fav cocrystal with all aromatic carboxylic acid coformers, viz., PABA, 4HBA, GA, and FRA, results in formation of an acid−amide heterodimer. On the other hand, the molecular analogue

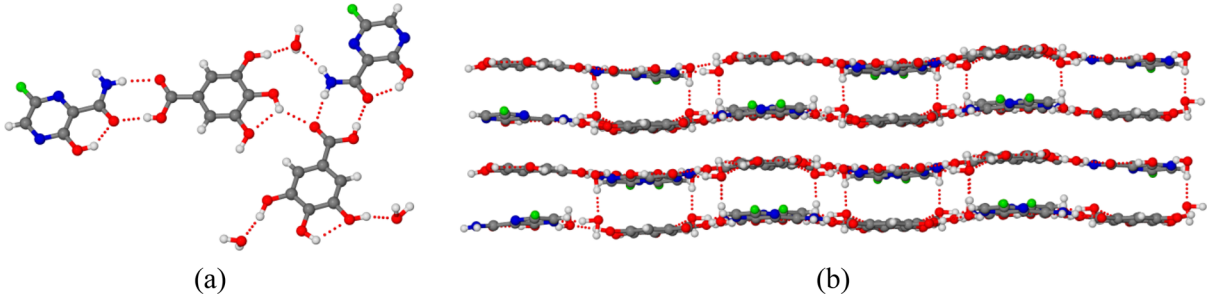

Figure 4. (a) Symmetry-independent Fav, GA, and two water molecules are connected to each other using N−H···O and O−H···O hydrogen bonds. (b) Crystal packing of Fav·GA·2H$_2$O cocrystal that shows layered crystal packing. Two symmetry-independent water molecules connect two layers through an O−H···O hydrogen bond.

https://doi.org/10.1021/acs.cgd.1c00339
Cryst. Growth Des. 2021, 21, 4417−4425

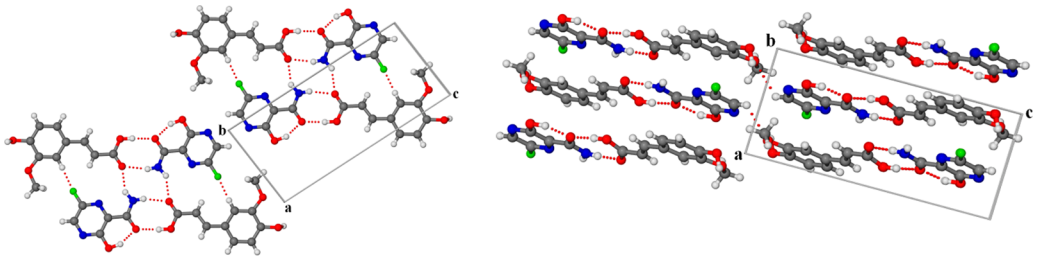

Figure 5. (a) Acid−amide dimer synthons connecting symmetry-independent Fav and FRA are shown. Adjacent Fav−FRA dimers are further connected via a bifurcated N−H···O hydrogen bond. (b) In 3D, discrete Fav−FRA dimers are stacked over each other in head-to-tail fashion.

Table 1. Crystallographic Parameters of Fav Cocrystals

	Fav·Theo (1:1)	Fav·PABA (1:1)	Fav·4HBA (1:1)	Fav·GA·2H_2O (1:1:2)	Fav·FRA (1:1)
chemical formula	$(C_5H_4FN_3O_2)\cdot(C_7H_8N_4O_2)$	$(C_5H_4FN_3O_2)\cdot(C_7H_7NO_2)$	$(C_5H_4FN_3O_2)\cdot(C_7H_6O_3)$	$(C_5H_4FN_3O_2)\cdot(C_7H_6O_5)\cdot 2(H_2O)$	$(C_5H_4F\ N_3O_2)\cdot(C_{10}H_{10}O_4)$
formula weight, M_r	337.29	294.25	295.23	363.26	351.29
crystal system	monoclinic	monoclinic	monoclinic	monoclinic	triclinic
space group	$P2_1/n$	$P2_1/c$	$P2_1/c$	$P2_1/n$	$P\bar{1}$
temperature (K)	296	296	296	296	296
a (Å)	13.407 (2)	7.5751 (8)	5.731 (2)	8.0991 (9)	6.8598 (7)
b (Å)	7.4694 (12)	13.4307 (14)	7.524 (3)	15.3276 (15)	7.3122 (7)
c (Å)	14.869 (2)	12.8854 (13)	28.525 (11)	12.1359 (13)	15.5320 (15)
α (deg)	90	90	90	90	95.006 (2)
β (deg)	107.834 (5)	92.582 (3)	94.428 (11)	94.539 (3)	91.089 (2)
γ (deg)	90	90	90	90	101.962 (2)
V (Å^3)	1417.5 (4)	1309.6 (2)	1226.3 (8)	1501.8 (3)	758.71 (13)
Z	4	4	4	4	2
radiation type	Mo Kα	Mo Kα	Mo Kα	Mo Kα	Mo Kα
μ (mm^{-1})	0.13	0.12	0.14	0.15	0.13
calc. density (g cm^{-3})	1.580	1.492	1.599	1.607	1.538
diffractometer	Bruker APEX-II CCD diffractometer	Bruker APEX-II CCD diffractometer	Bruker APEX-II CCD diffractometer	Bruker APEX-II CCD diffractometer	Bruker APEX-II CCD diffractometer
$R[F^2 > 2\sigma(F^2)]$	0.058	0.056	0.034	0.046	0.060
$wR(F^2)$	0.247	0.169	0.128	0.186	0.253
S	1.12	1.12	0.86	1.14	1.10
no. of reflections	2908	4039	2128	3053	4083
$\Delta\rho_{max}$, $\Delta\rho_{min}$ (e Å^{-3})	0.65, −0.65	0.66, −0.72	0.19, −0.20	0.50, −0.60	0.60, −0.70
CCDC number	2073033	2073034	2073030	2073032	2073031

pyrazinamide exhibits relatively rare isolated acid−acid and amide−amide homodimer synthons on cocrystallization with 4HBA[19] and FRA.[20] Saha and Desiraju[21] carried out a combinatorial study; tuning the chemical nature of acid and amide functionalities during cocrystallization resulted in the dominance of the acid−amide heterodimer synthon. Crystallographic information and hydrogen bond parameters of all the synthesized cocrystals are given in Tables 1 and 2, respectively.

Thermal Analysis. To examine the phase purity, Fav cocrystals were subjected to DSC measurements from 25 to 400 °C at a heating rate of 10 °C min^{-1}. No phase transitions were observed for any of the Fav cocrystals, and all of them showed a single and sharp melting endotherm different from the respective starting materials (see Table 3 and SI Figure S2). The DSC thermogram of Fav·GA powder material showed a broad endotherm peak at 116.5 °C (onset 96.6 °C, enthalpy 276.80 J/g) corresponding to the loss of two water molecules that is further confirmed using TG analysis that showed a weight loss of ∼10.08% (theoretical 9.91%) from 90 to 170 °C (see SI Figure S2g,h). Solvent loss at higher temperature compared to the boiling point of water signifies the presence of stronger hydrogen bond interactions between molecular counterparts and corresponding two water molecules in the crystal lattice. The TG curves of the rest of the cocrystals showed decomposition of the material after the melting event. In the case of Fav·Theo and Fav·FRA, decomposition is observed along with cocrystal dissociation based on first derivative of TG curves (see SI Figure S2).

Physicochemical Property Evaluation. As mentioned in the Introduction, there is no report on the physicochemical properties of Fav in the literature. Hence, investigation of physicochemical properties such as the stability as well as solubility of the synthesized cocrystals is of greater urge to better understand their efficacy as well as pharmacokinetic activity compared to the parent drug. Solubility analysis of the anhydrous form and all the synthesized cocrystals was carried out in distilled water as well as in pH 7 phosphate buffer using a shake-flask method[15] on the powder samples prepared using

https://doi.org/10.1021/acs.cgd.1c00339
Cryst. Growth Des. 2021, 21, 4417−4425

Table 2. Normalized Hydrogen Bond Metrics of Fav Crystal Structures

interaction	H···A (Å)	D···A (Å)	D−H···A (deg)	symmetry code
Fav·Theo (1:1)				
N6−H6A···O4	1.83	2.771(1)	150	−x + 2, −y, −z + 1
N3−H3B···O1	2.11	3.095(1)	159	−x + 2, −y + 1, −z + 2
N3−H3A···N7	2.15	3.118(1)	155	x, y, z
O2−H2A···O1	1.75	2.573(2)	145	x, y, z
C11−H11C···O1	2.57	3.629(1)	167	x − 1/2, −y + 1/2, +z − 1/2
C10−H10···O3	2.16	3.187(1)	159	x + 1/2, −y + 1/2, +z + 1/2
Fav·PABA (1:1)				
O2−H2A···O4	1.73	2.663(1)	170	x, y, z
N3−H3B···O3	1.97	2.979(1)	167	x, y, z
N3−H3A···N1	2.10	2.995(2)	144	x, −y + 1/2 + 1, +z − 1/2
N4−H4B···O3	2.01	3.028(1)	170	−x + 1, +y − 1/2, −z + 1/2
O1−H1A···O4	1.74	2.608(1)	152	x, y, z
C10−H10···O2	2.41	3.354(1)	145	x, −y + 1/2, +z − 1/2
N4−H4A···F1	2.32	3.260(1)	151	x − 1, +y − 1, +z
C3−H3···O4	2.43	3.458(1)	159	−x + 2, +y + 1/2, −z + 1/2 + 1
Fav·4HBA (1:1)				
N3−H3B···O3	1.90	2.908(1)	165	x, y, z
N3−H3A···O3	2.86	3.739(1)	144	−x, −y + 1, −z + 1
O4−H4A···O1	1.75	2.676(1)	167	x, y, z
O5−H5A···N2	2.02	2.947(1)	172	x, −y + 1/2, +z − 1/2
O2−H2A···O1	1.71	2.570(1)	150	x, y, z
C8−H8···F1	2.26	3.034(1)	127	−x, −y + 1, −z + 1
C3−H3···O2	2.36	3.292(1)	143	−x + 1, +y + 1/2, −z + 1/2 + 1
Fav·GA·2H_2O (1:1:2)				
O3−H3B···O1	1.71	2.636(1)	171	x, y, z
N3−H4A···O4	1.98	2.991(1)	168	x, y, z
O6−H6A···O4	2.27	2.971(1)	131	x + 1/2, −y + 1/2, +z − 1/2
O2−H2A···O1	1.81	2.618(1)	143	x, y, z
O7−H7A···$O8_w$	1.78	2.706(1)	170	x + 1, +y, +z
$O8_w$−H8B···O5	1.82	2.754(1)	174	x − 1/2, −y + 1/2, +z − 1/2
$O8_w$−H8A···N2	2.00	2.886(1)	156	x − 1/2, −y + 1/2 + 1, +z − 1/2
N3−H3A···$O9_w$	1.95	2.956(2)	166	x − 1/2, −y + 1/2 + 1, +z + 1/2
O5−H5A···$O9_w$	1.74	2.669(1)	174	x, +y − 1, +z
$O9_w$−H9A···$O8_w$	1.91	2.835(1)	168	−x + 1/2, +y + 1/2, −z + 1/2
$O8_w$−H8A···N2	2.00	2.886(1)	156	x − 1/2, −y + 1/2 + 1, +z − 1/2
C7−H7···O7	2.49	3.544(1)	166	x − 1/2, −y + 1/2, +z + 1/2
O2−H2A···F1	2.23	2.949(1)	133	x + 1/2, −y + 1/2 + 1, +z − 1/2
Fav·FRA (1:1)				
O4−H4A···O1	1.82	2.760(1)	176	x, y, z
N3−H3B···O3	1.84	2.838(1)	162	x, y, z
O2−H2A···O1	1.74	2.614(1)	154	x, y, z
N3−H3A···O3	2.24	3.093(1)	140	−x + 1, −y + 2, −z + 1
C7−H7···F1	2.39	3.350(1)	147	−x + 1, −y + 2, −z + 1
C15−H15B···O2	2.50	3.491(1)	152	x, +y, +z + 1

Table 3. Melting Point Peak Values of Fav Cocrystals and Respective Starting Materials

coformer	melting point (°C)	cocrystal	melting point peak (°C)
Fav tetragonal form[11]	192.5		
Fav orthogonal form[11]	190.7		
PABA	187	Fav·PABA	159.5
4HBA	214.5	Fav·4HBA	166.3
Theo	272	Fav·Theo	197.2
GA	260	Fav·GA·2H_2O	179.9
FRA	372.3	Fav·FRA	172.7

LAG. Prior to the solubility analysis, the bulk purity of the powder materials was confirmed using PXRD measurement (SI Figure S3). The solubility of the anhydrous form of Fav in distilled water/pH 7 phosphate buffer at room temperature (25 °C) was found to be 2.94/7.83 mg mL^{-1}. The equilibrium solubilities of all synthesized cocrystals in distilled water and pH 7 phosphate buffer medium are summarized in Figure 6. In the distilled water medium, cocrystals of Fav with PABA, 4HBA, and Theo showed enhanced solubility, whereas GA dihydrate and FRA cocrystals showed a decline in solubility compared to the Fav anhydrous form in the order Fav·PABA > Fav·4HBA > Fav·Theo > Fav > Fav·FRA > Fav·GA·2H_2O. In pH 7 phosphate buffer medium, there is an alteration in equilibrium solubility order, i.e, Fav·GA·2H_2O > Fav·Theo > Fav·PABA > Fav > Fav·4HBA > Fav·FRA. The alteration in solubility order is due to ionization of cocrystal components in buffer medium. The pH-dependent solubility of the cocrystal is well explored in the literature[22] and summarized in a review by Thakuria et al.[23] There are several factors that can affect the solubility/dissolution rate of multicomponent solids. Devarapalli et al. in a recent report[24] discusses the poor solubility of a hydrated salt−cocrystal of betrixaban based on the common ion effect. However, the presence of a less soluble coformer in the crystal lattice, a strong intermolecular interaction, the formation of hydrate, the pH of the dissolution media, the hydration rate, the particle size, the morphology of crystallites, etc. either alone or in combination also may influence the solubility/dissolution kinetics of APIs.[20,23,25−29] In our case,

https://doi.org/10.1021/acs.cgd.1c00339
Cryst. Growth Des. 2021, 21, 4417−4425

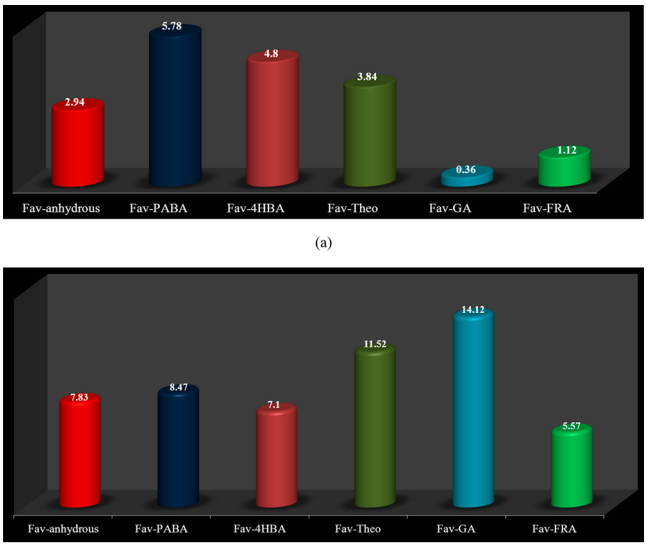

Figure 6. Bar diagram showing the equilibrium solubility of Fav and its cocrystals in (a) distilled water medium and (b) pH 7 phosphate buffer using a shake-flask method.

the trend in thermodynamic solubility of Fav cocrystals in distilled water medium nicely correlates with coformer solubility. Coformers with higher solubility resulted in an increase in the solubility of the associated cocrystals;[30] likewise, a decline in the solubility of Fav·FRA is due to the low solubility of FRA. The only exception observed in our study was Fav·GA·$2H_2O$ in distilled water medium. The low solubility of the corresponding cocrystal is due to the presence of two water molecules in the asymmetric unit. Water molecules present in the crystal lattice result in a decrease in solvation rate of the resultant cocrystal. The lower solubility of the hydrated cocrystal/salt compared to the anhydrous form is already well established in the literature.[31,32] The solubility trend in distilled water medium can also be explained based on the BFDH morphology prediction. As Fav·PABA and Fav·4HBA do not have any hydrophobic moiety, hydrophilic groups (amide, acid, amino, and hydroxyl) present in the crystal structure are exposed to the crystal surface, which can be solvated efficiently. Although, the Fav·Theo cocrystal has hydrophilic carbonyl and amine groups (Theo) exposed to the crystal surface, the presence of the two methyl groups (hydrophobic counterpart) decreases the solvation rate of the resultant cocrystal. Low solubility of the FRA cocrystal analogue was already elucidated in one of our previous reports.[29] The crystal morphology obtained during solution crystallization along with the BFDH predicted morphology of the Fav cocrystals are shown in SI Figure S5. Synthesized cocrystals of Fav were found to be quite stable and do not undergo dissociation/decomposition even at extreme conditions (water slurry for a period of ∼18 h/pH 7 phosphate buffer slurry for a period of ∼24 h), confirmed by comparing PXRDs of the slurry residues with freshly prepared LAG samples (see SI Figures S3 and S4). One interesting observation noticed during our investigation was the better moisture stability of the resultant Fav·Theo cocrystal based on PXRD measurement compared to the anhydrous form of Theo.[33,34] The PXRD of the slurry sample nicely matches with the calculated powder pattern of the Fav·Theo cocrystal, which suggests better stability of the cocrystal and does not dissociate into its starting materials or Theo monohydrate. Physical stability against atmospheric moisture is an important factor during processing, storage, and transportation of APIs in the pharmaceutical industry, which is addressed in a recent review.[35] From the SEM micrograph, it was observed that the particle sizes of Fav cocrystals are relatively smaller (∼400 nm to 2 μm) compared to the Fav anhydrous form (∼10 to 20 μm) (see SI Figure S6). The smaller particle size of cocrystals results in a larger surface area and higher solvation rate compared to the anhydrous form of Fav, which is observed in our case particularly for Fav·PABA, Fav·4HBA, and Fav·Theo cocrystals. The effect of particle size in material stability[36] as well as mechanical property[37] is well explored in the literature. Details of the solubility parameters of Fav cocrystals are listed in SI Tables S1−S3.

CONCLUSION

In this study, we have synthesized cocrystals of Fav with Theo and a few GRAS coformers using mechanochemistry[38,39] as well as solution crystallization. All the cocrystals were characterized comprehensively by SCXRD, PXRD, DSC, and TG analysis. In distilled water medium, we observed that the trend in cocrystal solubility nicely correlates with coformer solubility. An exceptionally low solubility of GA and FRA cocrystals could be explained based on formation of cocrystal dihydrate (in the case of Fav·GA·$2H_2O$) that restricts the rate of solvation and lower solubility of coformers (GA and FRA). Moreover, in pH 7 buffer medium, we observed a change in the trend of cocrystal solubility due to ionization of cocrystal components. Therefore, we can conclude that Fav cocrystal solubility can be tuned based on coformer selection during the cocrystallization process and pH of the medium. The newly synthesized drug−drug cocrystal Fav·Theo was found to have better solubility as well as stability compared to the parent drugs. Hence, the drug−drug cocrystal might be a potential formulation for patients suffering from a viral infection along with asthma or COPD related respiratory syndrome. This is one of the primary concerns for patients with respiratory syndrome or asthma suffering from COVID-19 infection. Moreover, the use of nutraceuticals such as FRA and GA as coformers may provide additional health benefits. As a limited number of studies on the efficacy of Fav against COVID-19 are reported in literature, in-depth biological study of Fav multicomponent solids might help to develop a better formulation with enhanced physicochemical properties in the near future. In order to minimize the time scale for drug approval for the treatment of new disease, increasing patent life and reducing the cost effect in drug development strategy, drug repurposing based on cocrystallization, preparation of polymorphs, fixed dose combination, nanoparticles, etc. has been the prime focus of global pharma industry as well as academia in the recent past.[40,41] We hope in the coming days, a greater number of reports on COVID-19 related drugs based on repurposing with improved efficacy will appear that might help to tackle this deadly virus.

ASSOCIATED CONTENT

Supporting Information

The Supporting Information is available free of charge at https://pubs.acs.org/doi/10.1021/acs.cgd.1c00339.

https://doi.org/10.1021/acs.cgd.1c00339
Cryst. Growth Des. 2021, 21, 4417−4425

Figure S1: PXRD of 1:1 Fav−GA ground powder compared with its starting materials. Figure S2: DSC and TGA thermograms of all Fav cocrystals. Tables S1−S3: Solubility parameters of the Fav anhydrous form and all synthesized Fav cocrystals. Figures S3 and S4: Comparison of PXRD patterns of solid residues obtained after solubility measurement with freshly prepared Fav cocrystals. Figure S5: BFDH morphology prediction of Fav cocrystals using Mercury software. Figure S6: SEM micrograph of the Fav anhydrous form and its cocrystals (PDF)

Accession Codes

CCDC 2073030−2073034 contain the supplementary crystallographic data for this paper. These data can be obtained free of charge via www.ccdc.cam.ac.uk/data_request/cif, or by emailing data_request@ccdc.cam.ac.uk, or by contacting The Cambridge Crystallographic Data Centre, 12 Union Road, Cambridge CB2 1EZ, UK; fax: +44 1223 336033.

AUTHOR INFORMATION

Corresponding Author

Ranjit Thakuria − *Department of Chemistry, Gauhati University, Guwahati 781014 Assam, India;* orcid.org/0000-0002-0325-3316; Email: ranjit.thakuria@gmail.com, ranjit.thakuria@gauhati.ac.in

Authors

Poonam Deka − *Department of Chemistry, Gauhati University, Guwahati 781014 Assam, India*

Diptajyoti Gogoi − *Department of Chemistry, Gauhati University, Guwahati 781014 Assam, India*

Khaled Althubeiti − *Department of Chemistry, College of Science, Taif University, Taif 21944, Saudi Arabia*

Dharmaraj R. Rao − *Research & Development Centre, Cipla Ltd, Mumbai 400083, India*

Complete contact information is available at: https://pubs.acs.org/10.1021/acs.cgd.1c00339

Author Contributions

‖P.D. and D.G. contributed equally to this study

Notes

The authors declare no competing financial interest.

ACKNOWLEDGMENTS

P.D. thanks the UGC for the Junior Research Fellowship (PhD scholar). K.A. thanks Taif University Researchers Supporting Project number (TURSP-2020/241), Taif University, Taif, Saudi Arabia. Favipiravir was a gift from Cipla, India. Dr. Yusuf K. Hamied, Chairman of Cipla Pharmaceuticals Ltd., is thanked for the scientific discussion, the Sophisticated Analytical Instrumentation Facility (SAIF), GU, is thanked for the use of the single crystal X-ray diffractometer, and the Department of Chemistry, GU, is thanked for the powder X-ray diffractometer, SEM, basic instrumentation facility, and infrastructure. We would also like to thank Dr. Tejender S. Thakur, CSIR-Central Drug Research Institute, Lucknow, for helpful discussions.

REFERENCES

(1) Shiraki, K.; Daikoku, T. Favipiravir, an anti-influenza drug against life-threatening RNA virus infections. *Pharmacol. Ther.* **2020**, *209*, 107512.

(2) Jin, Z.; Smith, L. K.; Rajwanshi, V. K.; Kim, B.; Deval, J. The ambiguous base-pairing and high substrate efficiency of T-705 (Favipiravir) Ribofuranosyl 5′-triphosphate towards influenza A virus polymerase. *PLoS One* **2013**, *8*, e68347−e68347.

(3) Sreekanth Reddy, O.; Lai, W.-F. Tackling COVID-19 Using Remdesivir and Favipiravir as Therapeutic Options. *ChemBioChem* **2021**, *22*, 939−948.

(4) Inoue, H.; Jinno, M.; Ohta, S.; Kishino, Y.; Kawahara, T.; Mikuni, H.; Sato, H.; Yamamoto, M.; Sato, Y.; Onitsuka, C.; Goto, Y.; Ikeda, H.; Sato, H.; Uno, T.; Uchida, Y.; Kimura, T.; Miyata, Y.; Hirai, K.; Homma, T.; Watanabe, Y.; Kusumoto, S.; Suzuki, S.; Tokimatsu, I.; Tanaka, A.; Sagara, H. Combination treatment of short-course systemic corticosteroid and favipiravir in a successfully treated case of critically ill COVID-19 pneumonia with COPD. *Respir. Med. Case Rep.* **2020**, *31*, 101200.

(5) Zhao, H.; Zhu, Q.; Zhang, C.; Li, J.; Wei, M.; Qin, Y.; Chen, G.; Wang, K.; Yu, J.; Wu, Z.; Chen, X.; Wang, G. Tocilizumab combined with favipiravir in the treatment of COVID-19: A multicenter trial in a small sample size. *Biomed. Pharmacother.* **2021**, *133*, 110825.

(6) Murohashi, K.; Hagiwara, E.; Kitayama, T.; Yamaya, T.; Higa, K.; Sato, Y.; Otoshi, R.; Shintani, R.; Okabayashi, H.; Ikeda, S.; Niwa, T.; Nakazawa, A.; Oda, T.; Okuda, R.; Sekine, A.; Kitamura, H.; Baba, T.; Komatsu, S.; Iwasawa, T.; Kaneko, T.; Ogura, T. Outcome of early-stage combination treatment with favipiravir and methylprednisolone for severe COVID-19 pneumonia: A report of 11 cases. *Respir. Investig.* **2020**, *58*, 430−434.

(7) Aktaş, A.; Tüzün, B.; Aslan, R.; Sayin, K.; Ataseven, H. New antiviral drugs for the treatment of COVID-19 instead of favipiravir. *J. Biomol. Struct. Dyn.* **2020**, 1−11.

(8) Bai, C.-Q.; Mu, J.-S.; Kargbo, D.; Song, Y.-B.; Niu, W.-K.; Nie, W.-M.; Kanu, A.; Liu, W.-W.; Wang, Y.-P.; Dafae, F.; Yan, T.; Hu, Y.; Deng, Y.-Q.; Lu, H.-J.; Yang, F.; Zhang, X.-G.; Sun, Y.; Cao, Y.-X.; Su, H.-X.; Sun, Y.; Liu, W.-S.; Wang, C.-Y.; Qian, J.; Liu, L.; Wang, H.; Tong, Y.-G.; Liu, Z.-Y.; Chen, Y.-S.; Wang, H.-Q.; Kargbo, B.; Gao, G. F.; Jiang, J.-F. Clinical and Virological Characteristics of Ebola Virus Disease Patients Treated With Favipiravir (T-705)—Sierra Leone, 2014. *Clin. Infect. Dis.* **2016**, *63*, 1288−1294.

(9) Shi, F.; Li, Z.; Kong, L.; Xie, Y.; Zhang, T.; Xu, W. Synthesis and crystal structure of 6-fluoro-3-hydroxypyrazine-2-carboxamide. *Drug Discoveries Ther.* **2014**, *8*, 117−120.

(10) Antonov, L. Favipiravir tautomerism: a theoretical insight. *Theor. Chem. Acc.* **2020**, *139*, 145.

(11) Goloveshkin, A. S.; Korlyukov, A. A.; Vologzhanina, A. V. Novel Polymorph of Favipiravir—An Antiviral Medication. *Pharmaceutics* **2021**, *13*, 139.

(12) Cherukuvada, S.; Thakuria, R.; Nangia, A. Pyrazinamide Polymorphs: Relative Stability and Vibrational Spectroscopy. *Cryst. Growth Des.* **2010**, *10*, 3931−3941.

(13) De Savi, C.; Hughes, D. L.; Kvaerno, L. Quest for a COVID-19 Cure by Repurposing Small-Molecule Drugs: Mechanism of Action, Clinical Development, Synthesis at Scale, and Outlook for Supply. *Org. Process Res. Dev.* **2020**, *24*, 940−976.

(14) Thakuria, R.; Sarma, B. Drug-Drug and Drug-Nutraceutical Cocrystal/Salt as Alternative Medicine for Combination Therapy: A Crystal Engineering Approach. *Crystals* **2018**, *8*, 101.

(15) Glomme, A.; März, J.; Dressman, J. B. Comparison of a miniaturized shake-flask solubility method with automated potentiometric acid/base titrations and calculated solubilities. *J. Pharm. Sci.* **2005**, *94*, 1−16.

(16) Sheldrick, G. A short history of SHELX. *Acta Crystallogr., Sect. A: Found. Crystallogr.* **2008**, *64*, 112−122.

(17) Atwood, J. L.; Barbour, L. J. Molecular Graphics: From Science to Art. *Cryst. Growth Des.* **2003**, *3*, 3−8.

(18) Barbour, L. J. X-Seed — A Software Tool for Supramolecular Crystallography. *J. Supramol. Chem.* **2001**, *1*, 189−191.

(19) Rajbongshi, T.; Sarmah, K. K.; Sarkar, A.; Ganduri, R.; Cherukuvada, S.; Thakur, T. S.; Thakuria, R. Preparation of Pyrazinamide Eutectics versus Cocrystals Based on Supramolecular Synthon Variations. *Cryst. Growth Des.* **2018**, *18*, 6640−6651.

(20) Sarmah, K. K.; Rajbongshi, T.; Bhowmick, S.; Thakuria, R. First-line antituberculosis drug, pyrazinamide, its pharmaceutically relevant cocrystals and a salt. *Acta Crystallogr., Sect. B: Struct. Sci., Cryst. Eng. Mater.* **2017**, *73*, 1007−1016.
(21) Saha, S.; Desiraju, G. R. Acid···Amide Supramolecular Synthon in Cocrystals: From Spectroscopic Detection to Property Engineering. *J. Am. Chem. Soc.* **2018**, *140*, 6361−6373.
(22) Chadha, R.; Saini, A.; Arora, P.; Jain, D. S.; Dasgupta, A.; Guru Row, T. N. Multicomponent solids of lamotrigine with some selected coformers and their characterization by thermoanalytical, spectroscopic and X-ray diffraction methods. *CrystEngComm* **2011**, *13*, 6271−6284.
(23) Thakuria, R.; Delori, A.; Jones, W.; Lipert, M. P.; Roy, L.; Rodríguez-Hornedo, N. Pharmaceutical cocrystals and poorly soluble drugs. *Int. J. Pharm.* **2013**, *453*, 101−125.
(24) Devarapalli, R.; Indukuri, A.; Bollineni, M.; Mondal, A.; Reddy, C. M.; Chennuru, R. Investigation of Poor Solubility of a Salt-Cocrystal Hydrate: A Case Study of the Common-Ion Effect in Betrixaban, an Anticoagulant Drug. *Mol. Pharmaceutics* **2021**, *18*, 1138−1149.
(25) Chen, Y. M.; Rodríguez-Hornedo, N. Cocrystals Mitigate Negative Effects of High pH on Solubility and Dissolution of a Basic Drug. *Cryst. Growth Des.* **2018**, *18*, 1358−1366.
(26) Maheshwari, C.; André, V.; Reddy, S.; Roy, L.; Duarte, T.; Rodríguez-Hornedo, N. Tailoring aqueous solubility of a highly soluble compound via cocrystallization: effect of coformer ionization, pHmax and solute−solvent interactions. *CrystEngComm* **2012**, *14*, 4801−4811.
(27) Sanphui, P.; Devi, V. K.; Clara, D.; Malviya, N.; Ganguly, S.; Desiraju, G. R. Cocrystals of Hydrochlorothiazide: Solubility and Diffusion/Permeability Enhancements through Drug−Coformer Interactions. *Mol. Pharmaceutics* **2015**, *12*, 1615−1622.
(28) Sarmah, K. K.; Nath, N.; Rao, D. R.; Thakuria, R. Mechanochemical synthesis of drug−drug and drug−nutraceutical multicomponent solids of olanzapine. *CrystEngComm* **2020**, *22*, 1120−1130.
(29) Sarmah, K. K.; Boro, K.; Arhangelskis, M.; Thakuria, R. Crystal structure landscape of ethenzamide: a physicochemical property study. *CrystEngComm* **2017**, *19*, 826−833.
(30) Saraswatula, V. G.; Bhat, M. A.; Gurunathan, P. K.; Saha, B. K. Comparison of pyridyl and pyridyl N-oxide groups as acceptor in hydrogen bonding with carboxylic acid. *CrystEngComm* **2014**, *16*, 4715−4721.
(31) Bartolomei, M.; Bertocchi, P.; Antoniella, E.; Rodomonte, A. Physico-chemical characterisation and intrinsic dissolution studies of a new hydrate form of diclofenac sodium: comparison with anhydrous form. *J. Pharm. Biomed. Anal.* **2006**, *40*, 1105−1113.
(32) Aaltonen, J.; Heinänen, P.; Peltonen, L.; Kortejärvi, H.; Tanninen, V. P.; Christiansen, L.; Hirvonen, J.; Yliruusi, J.; Rantanen, J. In situ measurement of solvent-mediated phase transformations during dissolution testing. *J. Pharm. Sci.* **2006**, *95*, 2730−2737.
(33) Rodríguez-Hornedo, N.; Lechuga-Ballesteros, D.; Wu, H.-J. Phase transition and heterogeneous/epitaxial nucleation of hydrated and anhydrous theophylline crystals. *Int. J. Pharm.* **1992**, *85*, 149−162.
(34) Zhu, H.; Yuen, C.; Grant, D. J. W. Influence of water activity in organic solvent + water mixtures on the nature of the crystallizing drug phase. 1. Theophylline. *Int. J. Pharm.* **1996**, *135*, 151−160.
(35) Thakur, T. S.; Thakuria, R. Crystalline Multicomponent Solids: An Alternative for Addressing the Hygroscopicity Issue in Pharmaceutical Materials. *Cryst. Growth Des.* **2020**, *20*, 6245−6265.
(36) Thakuria, R.; Arhangelskis, M.; Eddleston, M. D.; Chow, E. H. H.; Sarmah, K. K.; Aldous, B. J.; Krzyzaniak, J. F.; Jones, W. Cocrystal Dissociation under Controlled Humidity: A Case Study of Caffeine−Glutaric Acid Cocrystal Polymorphs. *Org. Process Res. Dev.* **2019**, *23*, 845−851.
(37) Karunatilaka, C.; Bučar, D.-K.; Ditzler, L. R.; Friščić, T.; Swenson, D. C.; MacGillivray, L. R.; Tivanski, A. V. Softening and Hardening of Macro- and Nano-Sized Organic Cocrystals in a Single-Crystal Transformation. *Angew. Chem., Int. Ed.* **2011**, *50*, 8642−8646.
(38) Tan, D.; Loots, L.; Friščić, T. Towards medicinal mechanochemistry: evolution of milling from pharmaceutical solid form screening to the synthesis of active pharmaceutical ingredients (APIs). *Chem. Commun.* **2016**, *52*, 7760−7781.
(39) James, S. L.; Adams, C. J.; Bolm, C.; Braga, D.; Collier, P.; Friščić, T.; Grepioni, F.; Harris, K. D. M.; Hyett, G.; Jones, W.; Krebs, A.; Mack, J.; Maini, L.; Orpen, A. G.; Parkin, I. P.; Shearouse, W. C.; Steed, J. W.; Waddell, D. C. Mechanochemistry: opportunities for new and cleaner synthesis. *Chem. Soc. Rev.* **2012**, *41*, 413−447.
(40) Mullard, A. Drug repurposing programmes get lift off. *Nat. Rev. Drug Discovery* **2012**, *11*, 505−506.
(41) Parvathaneni, V.; Kulkarni, N. S.; Muth, A.; Gupta, V. Drug repurposing: a promising tool to accelerate the drug discovery process. *Drug Discovery Today* **2019**, *24*, 2076−2085.

https://doi.org/10.1021/acs.cgd.1c00339
Cryst. Growth Des. 2021, 21, 4417−4425